



Flavonol-mediated stabilization of PIN efflux complexes regulates polar auxin transport

William D Teale^{1,*} , Taras Pasternak¹, Cristina Dal Bosco¹, Alexander Dovzhenko¹ , Krystyna Kratzat¹, Wolfgang Bildl², Manuel Schwörer¹, Thorsten Falk³, Benadetto Rupert⁴, Jonas V Schaefer⁵, Mojgan Shahriari¹, Lena Pilgermayer¹, Xugang Li⁶, Florian Lübben¹ , Andreas Plückthun⁵ , Uwe Schulte^{2,7,8} & Klaus Palme^{1,8,**} 

Abstract

The transport of auxin controls the rate, direction and localization of plant growth and development. The course of auxin transport is defined by the polar subcellular localization of the PIN proteins, a family of auxin efflux transporters. However, little is known about the composition and regulation of the PIN protein complex. Here, using blue-native PAGE and quantitative mass spectrometry, we identify native PIN core transport units as homo- and heteromers assembled from PIN1, PIN2, PIN3, PIN4 and PIN7 subunits only. Furthermore, we show that endogenous flavonols stabilize PIN dimers to regulate auxin efflux in the same way as does the auxin transport inhibitor 1-naphthylphthalamic acid (NPA). This inhibitory mechanism is counteracted both by the natural auxin indole-3-acetic acid and by phosphomimetic amino acids introduced into the PIN1 cytoplasmic domain. Our results lend mechanistic insights into an endogenous control mechanism which regulates PIN function and opens the way for a deeper understanding of the protein environment and regulation of the polar auxin transport complex.

Keywords Auxin; efflux; flavonol; inhibition; MFS

Subject Categories Membrane & Trafficking; Plant Biology

DOI 10.15252/emj.2020104416 | Received 7 January 2020 | Revised 4

September 2020 | Accepted 6 October 2020 | Published online 13 November 2020

The EMBO Journal (2021) 40: e104416

Introduction

In plants, concentration gradients of auxin direct cell identity and growth (Benkova *et al.*, 2003). Although PIN auxin efflux carriers, polarly localized major facilitator superfamily (MFS) proteins,

establish these gradients in response to developmental and environmental cues, they are not solely responsible for the regulated transport of auxin out of the cell (Paponov *et al.*, 2005; Geisler *et al.*, 2016).

For many years, specific inhibitors have played a key role in the identification and characterization of the wider polar auxin transport (PAT) machinery (Morgan & Soding, 1958; Hertel *et al.*, 1983). One such compound, 1-naphthylphthalamic acid (NPA), inhibits a second group of dedicated auxin efflux carriers belonging to the ABCB family of multidrug efflux proteins. NPA disrupts the association between ABCB19 and the immunophilin-like FKBP42 TWISTED DWARF1 (TWD1) (Bailey *et al.*, 2008); however, several lines of evidence suggest that this interaction is not the only way in which NPA inhibits PAT.

The complicated nature of cellular auxin efflux regulation is illustrated by the observation that NPA-treated plants resemble the *pin1* but not the *abcb19* phenotype in diverse species (Katekar & Geisler, 1980; Okada *et al.*, 1991; Reinhardt *et al.*, 2000; Xu *et al.*, 2005). Furthermore, NPA binds to ABCB proteins at a concentration of 10 nM, (Zhu *et al.*, 2016) but only inhibits auxin transport when present in excess of 100 nM (Michalke *et al.*, 1992). Thirdly, in *Arabidopsis*, *abcb19* and *pin1* both display reductions in basipetal auxin transport capacity of over 50% when compared to wild type (Okada *et al.*, 1991; Noh *et al.*, 2001), implying that their mechanisms at least partially overlap. Indeed, the proteins have been shown to interact in plants, with ABCB19 stabilizing PIN1 in specific membrane microdomains (Titapiwatanakun *et al.*, 2009) lending weight to the hypothesis that they both represent components of a common auxin efflux protein complex (Blakeslee *et al.*, 2007). The ability of PIN1 and ABCB19 together to stimulate cellular auxin efflux in an NPA-sensitive manner has been demonstrated after their co-expression in human cells (Rojas-Pierce *et al.*, 2007). However, to date, no careful characterization of the stoichiometry of native PIN1/ABCB19-containing protein complexes has been carried out.

1 Institute of Biology II, University of Freiburg, Freiburg, Germany

2 Institute of Physiology II, Faculty of Medicine, University of Freiburg, Freiburg, Germany

3 Institute for Computer Science, University of Freiburg, Freiburg, Germany

4 Department of Agronomy, Food, Natural resources, Animals and Environment—DAFNAE, University of Padova, Padova, Italy

5 High-Throughput Binder Selection Facility, Department of Biochemistry, University of Zurich, Zurich, Switzerland

6 Sino German Joint Research Center for Agricultural Biology, and State Key Laboratory of Crop Biology, College of Life Sciences, Shandong Agricultural University, Tai'an, China

7 Logopharm GmbH, Freiburg, Germany

8 Signalling Research Centres BIOS and CIBSS, Freiburg, Germany

*Corresponding author. Tel: +49 761 20367861; E-mail: william.teale@biologie.uni-freiburg.de

**Corresponding author. Tel: +49 761 2032954; E-mail: klaus.palme@biologie.uni-freiburg.de

ABCB19 interacts with TWD1 in the absence of NPA with the function of this interaction appearing to be related to the proper trafficking of ABCB19 to the plasma membrane (Bailly *et al.*, 2008; Wu *et al.*, 2010). However, despite such detailed insights, an overall understanding of the relationship between NPA and the auxin efflux complex remains elusive (Geisler *et al.*, 2016). Two NPA-binding sites of low and high affinity at the plasma membrane have been proposed, but it is the estimated dissociation constant of the low-affinity site (approximately 1 μ M) which correlates closely with the concentration of NPA which inhibits auxin efflux (Michalke *et al.*, 1992). However, it is ABCB19 (with a relatively high affinity for NPA) and not PIN1 (not a high-affinity NPA-binding protein) which has been shown most convincingly to be the target for NPA-mediated auxin transport inhibition.

NPA is a particularly important inhibitor as it gives easy experimental access to an endogenous mechanism which regulates PAT. It does this by competing for membrane-binding sites with flavonols such as kaempferol and quercetin (Rubery, 1990). In general, those flavonols which most efficiently inhibit auxin transport also show the greatest ability to displace NPA from cell membranes (Jacobs & Rubery, 1988), and *tt4*, an Arabidopsis genotype unable to synthesize flavonols, displays higher rates of PAT (Buer *et al.*, 2013). Although the currently available data suggest that flavonols inhibit ABCB-mediated auxin efflux (Geisler *et al.*, 2005), they also indicate that this interaction is embedded into a more intricate regulatory mechanism, possibly also involving the direct inhibition of MFS proteins.

In this report, we investigate the relationship between NPA and the PIN proteins, showing that (i) NPA directly inhibits PIN1-mediated cellular auxin efflux, (ii) the functional core of the PIN protein complex contains only trace amounts of ABCB proteins, but (iii) comprises a PIN dimer which is stabilized by both NPA and flavonols, and (iv) this stabilization is necessary for the inhibition of PIN-mediated auxin efflux by NPA and flavonols, thus revealing a crucial regulatory mechanism.

Results

In order to establish whether NPA is able to inhibit PIN1-dependent cellular auxin efflux in plants, an efflux assay was designed in which a nuclear auxin sensor was co-expressed with PIN1 in Arabidopsis leaf protoplasts (Wend *et al.*, 2013). Here, auxin-mediated degradation of an AUX/IAA domain II-linked firefly luciferase sensor, normalized with a translationally fused Renilla luciferase, enabled the relative quantification of internal auxin concentration between populations of cells incubated in solutions containing different concentrations of the natural auxin, indole-3-acetic acid (IAA). These measurements enabled the relative efflux capacity of the cells to be inferred. All assay conditions have been previously optimized elsewhere (Wend *et al.*, 2013). In untransformed cells, NPA did not significantly alter the accumulation of intracellular IAA (as measured by the stabilization of firefly luciferase activity) when protoplasts were incubated in external IAA concentrations ranging between 1 nM and 10 μ M, indicating that no NPA-sensitive background auxin transport activity could be measured. However, PIN-dependent IAA efflux, which counteracted the intracellular accumulation of IAA, occurred in protoplasts transiently expressing PIN1 after incubation in IAA solutions at

concentrations higher than 1 nM (Fig 1A). This activity of PIN1 was largely inhibited by the application of NPA, over nearly the whole range of IAA concentrations investigated (Fig 1A).

An NPA concentration of around 5 μ M was sufficient to fully inhibit PIN1-dependent auxin transport in this system (Fig 1B). These values correspond well with both the K_d of the interaction between NPA and the low-affinity microsomal NPA-binding site (Michalke *et al.*, 1992) and the concentrations at which NPA inhibits PAT in plants (Hertel & Leopold, 1962). We therefore conclude that in its native environment of the plant plasma membrane, PIN1 is able to effect the cellular efflux of IAA, and this efflux is inhibited by NPA.

PINs are not the only plant proteins which transport auxin in an NPA-sensitive manner. ABCB19, ABCB1 and ABCB21-dependent auxin efflux are also inhibited by NPA, and knockout plants have a reduced capacity for PAT (Noh *et al.*, 2001; Bailly *et al.*, 2008; Jenness *et al.*, 2019). As ABCB19 has previously been shown to interact with PIN1 (Blakeslee *et al.*, 2007), we set out to test specifically whether ABCB19 and PIN1 were core components of the same complex. As a first approach, Arabidopsis plasma membrane proteins were solubilized under low (ComplexioLyte 47 [CL47]) or high (ComplexioLyte 27 [CL27]) stringency conditions (optimized mixtures of non-ionic and partially ionic detergents, respectively; Logopharm GmbH) and resolved by blue-native polyacrylamide gel electrophoresis (BN-PAGE). An optimum solubilization protein-detergent ratio of 1:7 (w/w) was determined in titration experiments to exclude size shift artefacts that could result from incomplete solubilization (Fig EV1A). Subsequent SDS-PAGE separation showed PIN1 to be a constituent of a homogenous protein complex focusing at an apparent molecular size of around 350 kDa at low stringency (Fig 2A). Upon more stringent solubilization with CL27, dissociation into smaller subcomplexes occurred, with more dispersed populations of PIN1 detected at between 100 kDa and 300 kDa (Fig 2B).

To identify the protein composition of the larger, low stringency-solubilized PIN assembly, we affinity-purified GFP-fused PIN proteins from Arabidopsis roots after expression from their native promoters and after the induction of discrete lateral roots and analysed the captured proteins by label-free quantitative mass spectrometry (LC-MS/MS). This approach included GFP-PINs 1, 3, 4 and 7 proteins, which are all exclusively localized to the plasma membrane, share similar expression domains and display considerable functional redundancy in the Arabidopsis root apical meristem, as well as GFP-PIN2 (Blilou *et al.*, 2005). Proteins were solubilized and subjected to affinity purification (AP) with an immobilized anti-GFP monoclonal antibody or GFP-specific designed ankyrin repeat protein (DARPin) (Dreier *et al.*, 2011; Brauchle *et al.*, 2014); the DARPin, a small, stable GFP-binding protein, significantly outperformed more traditional antibody-based purifications in our analysis. Proteins that bound a negative control bait protein (the plasma membrane-bound LTI6b-GFP) in a parallel experiment were not considered as PIN interactors. Under these conditions, all GFP-tagged PIN proteins could be purified together with lesser amounts of endogenous untagged PIN subtypes and a limited set of other proteins including PGP19 (Fig EV1B). Determination of molecular abundance using concatenated protein standards for peptide intensity calibration (label-free QconCAT (Schwenk *et al.*, 2014)) confirmed that PIN1-GFP co-purified only substoichiometric amounts of endogenous PINs and PGP19 (Fig 2C). These results suggest that native PIN 1, 2, 3, 4 and 7 core complexes may exist as detergent-

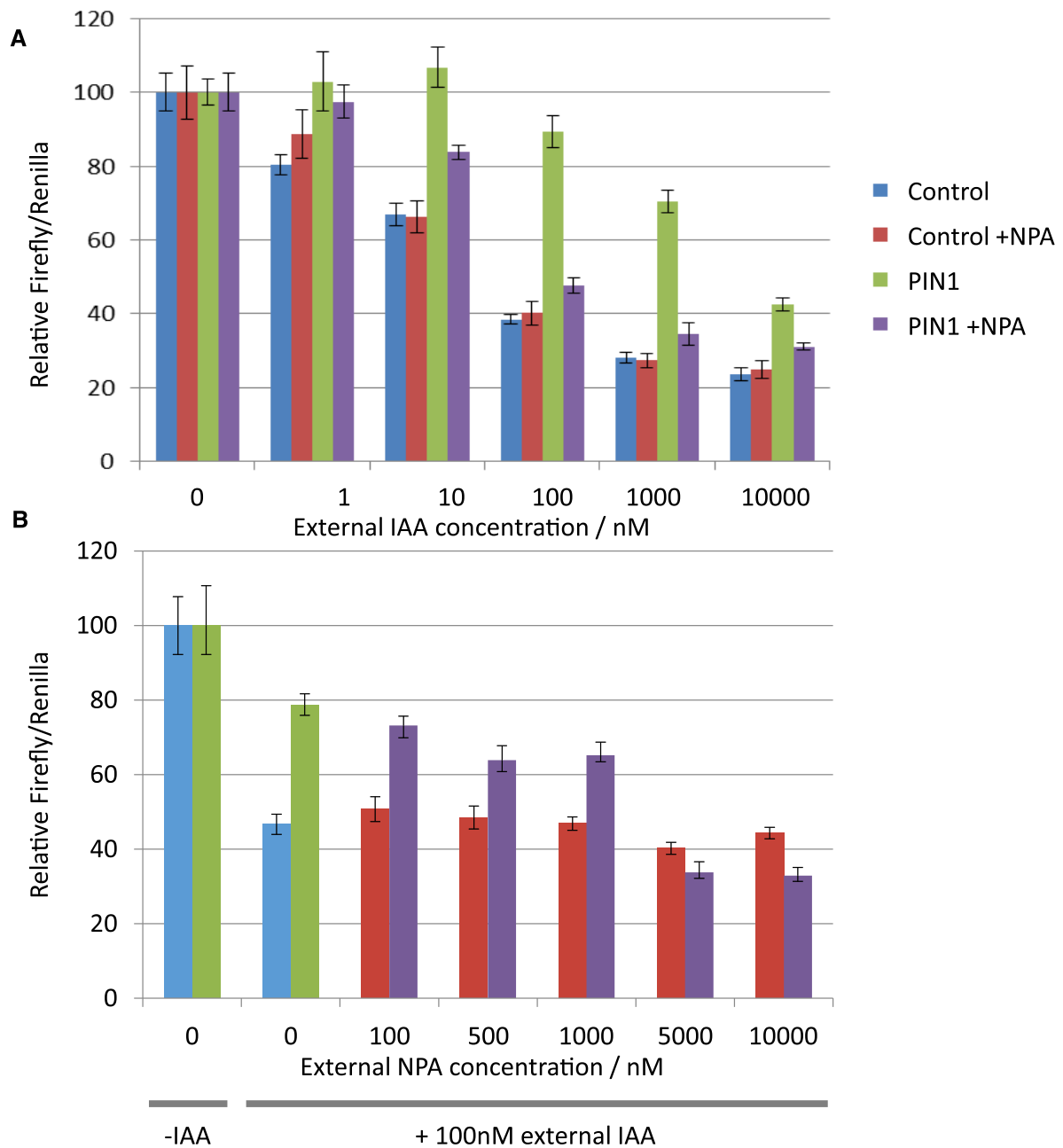


Figure 1. NPA inhibits PIN1-dependent cellular auxin efflux.

A Normalized firefly luciferase luminescence (compared to Renilla luciferase) as a function of external IAA concentration. Arabidopsis protoplast cells were transiently transformed with either AtPIN1 or GFP (in the case of the control) both under the control of a constitutive CaMV 35S promoter. Where indicated, 10 μ M NPA was added. **B** Normalized firefly luciferase luminescence (compared to Renilla luciferase) as a function of external NPA concentration in the presence of 100nM IAA in control GFP (blue or red)- or PIN1 (green or purple)-transformed protoplasts.

Data information: Each point is the mean of six measurements normalized to the firefly luciferase signal from cells with no external auxin added. $n = 6$, error bars indicate standard error.

labile dimers or tetramers in mostly homomeric configuration which do not contain PGP19. Formation of PIN1 heteromers was recapitulated by pull-down of either 3xHis-tagged PIN1 or PIN3 together with GFP-PIN1, after all constructs were transiently expressed in

tobacco leaves (Fig EV1C and D). Endogenous PIN1 was detected in Western blots of PIN1-GFP (where the band intensities between PIN1 and PIN1-GFP proteins were similar), PIN3-GFP, PIN4-GFP and PIN7-GFP (Fig EV1B, lower panel).

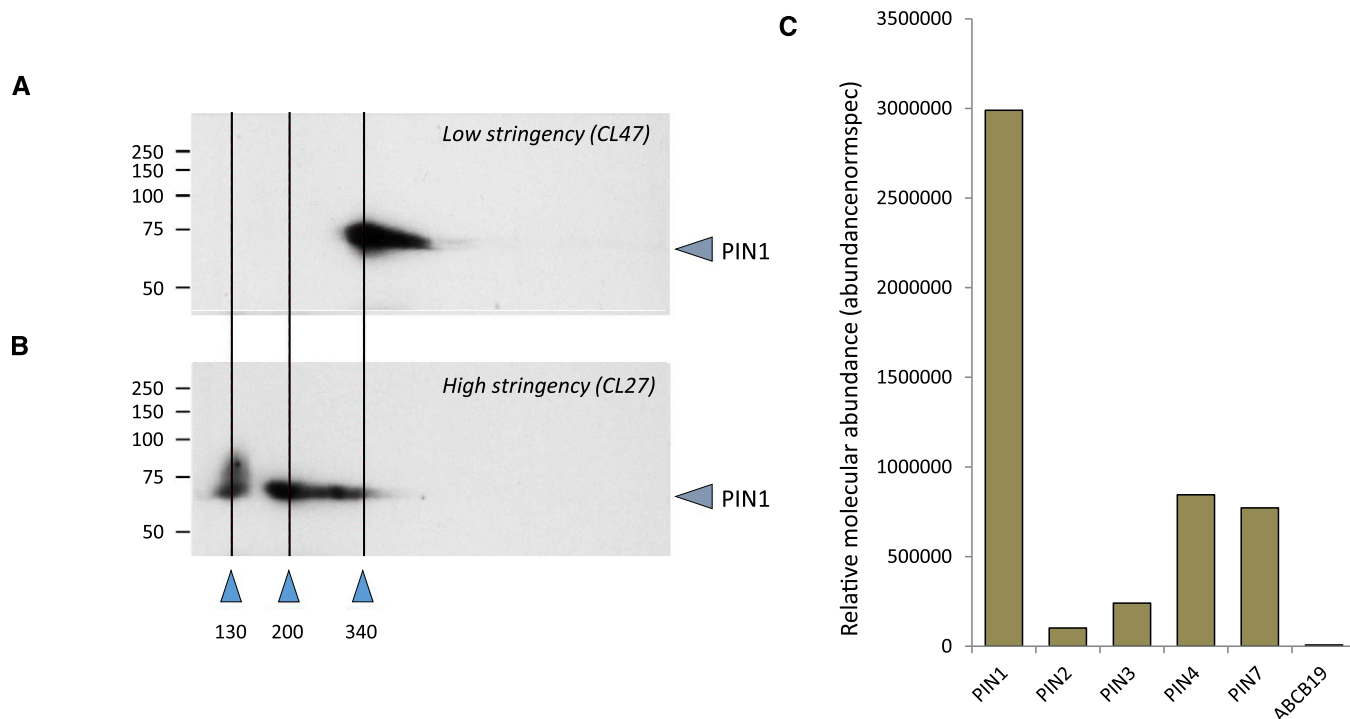


Figure 2. Definition and composition of the PIN1 core complex.

- A, B Native PAGE separation reveals distinct detergent-sensitive PIN1 complexes. Plasma membrane preparations from dark-grown *Arabidopsis* cell suspension cultures were solubilized with (A) ComplexioLyte 27 (a mixture of ionic and non-ionic detergents) and (B) ComplexioLyte 47 (lower stringency, non-ionic detergent) (both Logopharm); first dimension BN-PAGE, second dimension SDS-PAGE, blots stained with anti-PIN1 antibody revealing distinct PIN1 complex populations at the indicated positions. Values are given in kDa.
- C Molecular abundance (abundancenormspec values calculated as summarized peptide PVs divided by the number of MS-accessible protein-specific amino acids) of PIN subunits and ABCB19 in anti-GFP affinity purification of CL47-solubilized PIN1-GFP-expressing roots with a GFP-specific DARPIn. Note the significant heteromerization of several endogenous PINs with PIN1-GFP and the absence of other abundant interaction partners (ABCB19 shown as an example).

We next tested whether PIN1 complex formation was independent from other plant factors by heterologous reconstitution of the PIN1 complex in a human cell line. BN-PAGE analysis of PIN1-transfected HEK cells solubilized with CL27 showed two PIN1 signals, one at 100 kDa representing PIN1 monomers and one around 230 kDa likely resulting from PIN1 dimers (Fig 3A). However, PIN1 dimer formation/stability was significantly less in HEK cells than in *Arabidopsis* microsomes, prepared from MM2d cells, a dark-grown *Arabidopsis* cell culture consistently able to yield large amounts of homogenous material (Menges *et al*, 2002). We therefore hypothesized the existence of a plant-specific factor which stabilized PIN1 dimers.

We next tested the influence of various auxin transport inhibitors and modulators of IAA transport on the stability of solubilized PIN1 dimers. Incubation of PIN1-expressing HEK membranes with 10 μ M NPA or the flavonol quercetin (also at 10 μ M), an endogenous functional analogue of NPA (Brown *et al*, 2001), prior to solubilization stabilized the PIN1 complex at 230 kDa, an identical size to the PIN1 complex found in plants and solubilized under identical conditions (Fig 3A). We therefore conclude that, in plants, the core PIN1 complex comprises flavonol-stabilized PIN dimers.

Further experiments showed that naturally occurring flavonols varied in their ability to stabilize PIN interactions, but incubation with quercetin glycoside, a related compound which does not inhibit PAT,

did not stabilize PIN1 dimers (Appendix Fig S1) (Jacobs & Rubery, 1988). The specificity of dimer stabilization was next tested as plant-derived microsome preparations were incubated with a range of compounds prior to their solubilization. As shown in Appendix Fig S2, at 50% CL27, PIN1 was distributed between 230 kDa complex and a monomer migrating at 100 kDa. However, in the presence of 10 μ M NPA, PIN1 was localized exclusively to the 230 kDa complex. At concentrations of 10 μ M, incubation in the presence of tryptophan, the PAT inhibitor 2,3,5 triiodobenzoic acid (TIBA) or the exocytosis inhibitor brefeldin A (BFA) did not alter the distribution of PIN1 between the 230 kDa and 100 kDa populations. We therefore conclude that the stabilization of the endogenous PIN1 auxin efflux core complex is specifically dependent on NPA and the PAT-inhibiting flavonols to which it is functionally related.

To test whether this stabilization was specific to PIN1, we transiently expressed PIN4 in HEK293 cells before incubation with NPA, which resulted in the stabilization of PIN4 protein complexes (Appendix Fig S1). The stabilization of protein interactions by NPA is therefore likely to be a shared feature within the PIN1, PIN2, PIN3, PIN4 and PIN7 subfamily (Paponov *et al*, 2005).

The regulation of function by substrate concentration is an established model of transporter feedback control (Zahniser & Doolen, 2001). We therefore wanted to know whether IAA effected its own

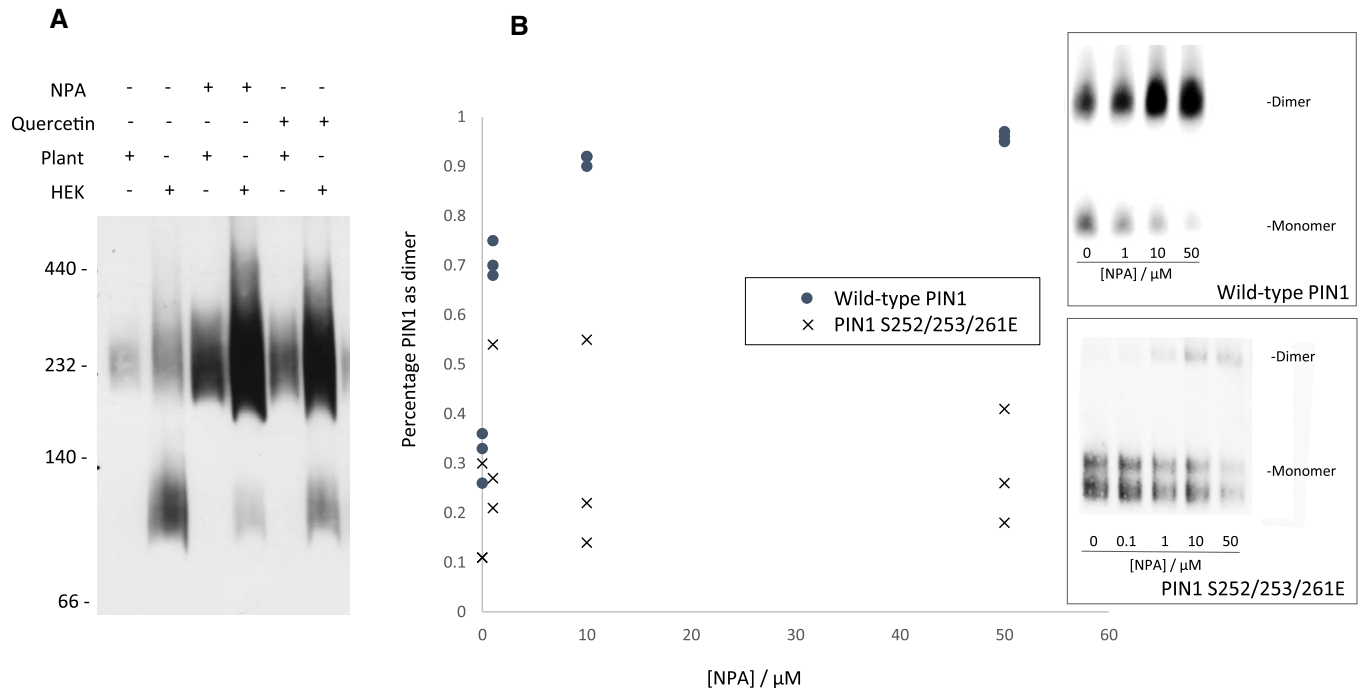


Figure 3. NPA and quercetin both stabilize PIN1 complex formation.

A BN-PAGE was performed with PIN1-containing microsomes prepared from either PIN1-expressing HEK293T cells or a dark-grown *Arabidopsis* cell suspension culture. Prior to solubilization with 1% dodecyl maltoside, microsomes were incubated with either 10 μ M NPA or 10 μ M quercetin.

B PIN1 dimer stability induced by NPA after expression in HEK cells. Relative distribution between monomer and dimer after NPA treatment is given relative to distribution of untreated samples after solubilization with 50% (v/v) CL27. Each measurement given (three for each concentration) represents the mean of three gel lanes for wild type (circles) or triple S252S, S253E and S261E phosphomimetic sequences (crosses) (example images are given in the figure inset).

efflux by counteracting the ability of NPA to stabilize PIN-PIN interactions (Paciorek *et al*, 2005). To this end, microsomes from HEK cells expressing PIN1 were solubilized and BN-PAGE was separated in the presence of IAA and NPA (Fig EV2A). PIN1 dimers were stabilized from 1 μ M NPA. However, in the presence of IAA, the lowest concentration at which PIN1 dimers were observed was 6 μ M NPA. At 10 μ M NPA, the proportion of preserved PIN1 dimers was decreased by the addition of IAA (Fig EV2A). The presence of 10 μ M IAA inhibited NPA-induced dimer stabilization, a process which was sensitive at a lower NPA concentration (Fig EV2B). We therefore conclude that IAA and NPA are able to act in an antagonistic manner on the stability of PIN1 dimers.

The cytosolic domain of PIN1 is reversibly phosphorylated by AGC kinases at several positions (Michniewicz *et al*, 2007). The consequence of this phosphorylation is twofold: it changes the apical-basal polarity of the plasma membrane localization (Friml *et al*, 2004) and increases the rate of auxin efflux (Zourelidou *et al*, 2014). We therefore next introduced residues to mimic phosphorylated serine residues to test whether phosphorylation of the PIN1 cytosolic domain could lead to dimer instability. Three phosphoserines were identified in the PIN1 cytosolic domain in our MS/MS analysis of the affinity-purified solubilized PIN1 complex: Ser252, Ser253 and Ser261. After replacing each with glutamic acid, the full-length PIN1 sequences were expressed in HEK cells, and protein extracts were treated with NPA and solubilized as described above. 50 μ M NPA failed to fully stabilize dimers of PIN1 proteins carrying

phosphomimetic point mutations at all concentrations tested (Fig 3B). These data support the hypothesis that PIN1 phosphorylation functions, at least in part, by reducing the affinity with which core complexes enter into a stable inactive conformation.

In order to ascertain whether PIN dimer stability can be regulated in living plants, PIN interactions in *Arabidopsis* root meristems were measured with a quantitative 3-D proximity ligation assay (PLA; Pasternak *et al*, 2018) after the exogenous application of NPA and IAA (both at 10 μ M). Proximity ligation assays use complementary oligonucleotides fused to antibodies to determine the frequency with which proteins of interest find themselves in close proximity. A matrix of PIN interactions was tested in order to assess the reliability of the assay in *Arabidopsis* roots, with the prediction that fewer interactions should occur when target protein pairs have increasingly discrete expression domains (Fig EV3).

No PLA interactions were observed for the PIN1 and PIN3 pair; the expression domain of these proteins does not overlap in the root apical meristem (Fig EV3A and G). Conversely, PIN3 and PIN4 share highly similar expression domains and displayed a relatively high density of PLA interactions (Fig EV3F and L). In all cases tested, the density of PLA interactions correlated well with the size of the co-expression domain independent of assay orientation (Fig EV3B-E and G-K). PIN1-PIN2 interactions were only observed when PIN1 expression was driven within PIN2 domains by the constitutive 35S promoter (PIN1 and PIN2 occupy largely non-overlapping expression domains), and PIN1 was strongly labelled

when both (+) and (–) PLA oligonucleotides were coupled to different populations of anti-PIN1 antibodies (Fig EV3M–P). Interactions between PIN1 and either LTI6b-GFP or an H⁺ATPase were measured at very low densities (Fig EV3Q and R).

In order to test whether NPA and IAA affected the degree of PIN heterodimerization *in planta*, the PIN1-PIN4 PLA interaction was analysed as it occurred at an intermediate frequency between abundant (e.g. PIN3-PIN4) and rare (e.g. PIN1-PIN3) interactions and thus left scope for us to measure either an increase or a decrease in the density of interaction events. To compare accurately the localization of protein–protein interactions among populations of roots, iRoCS, an intrinsic root coordinate system, was used to annotate fully and accurately overlay the RAM of the root in 3D with respect to the positions of cells, protein–protein interactions and expression domains (Schmidt *et al*, 2014). In the untreated RAM (excluding root cap and columella cells), an average of 697 (s.d. = 125) PIN1-PIN4 interactions was detected ($n = 3$; Fig 4; Appendix Fig S3).

The spatial distribution of PLA spots overlapped with the PIN1-PIN4 co-localization domain (Fig 4A). After incubation with 10 μ M NPA for 30 min, an average of 1,061 (s.d. = 123) interactions was detected in the same region. In contrast, the application of IAA caused a reduction in PIN1-PIN4 proximity, with 320 (s.d. = 95) interactions detected. However, when seedlings were incubated simultaneously with NPA and IAA, the number of interactions returned to a similar frequency as was observed for untreated roots (498; s.d. = 181; Fig 4B). These data indicate that, in agreement with *in vitro* data, IAA and NPA have antagonistic effects on the stability of PIN1-PIN4 complexes *in planta*. The NPA-dependent stabilization of PIN1-PIN4 dimerization therefore increased the overall number of interactions in the root meristem.

The distribution of PIN1-PIN4 interactions remained relatively constant among cell layers in all treatments, with the frequency of interactions within 50 μ m of the quiescent centre (QC) (where new cell files originate) being relatively insensitive (Fig 4B). For example, interactions in cells further than 50 μ m from the QC differed by 573 between IAA and NPA treatments, compared to only 168 within 50 μ m of the QC between the same treatments. The difference between treatments is therefore largely due to the effect of treatments on PIN complexes which lie further than 50 μ m from the QC. These data support existing evidence that endogenous suppression of PAT by flavonols occurs primarily in elongating rather than dividing cells (Peer *et al*, 2001). Taken together, these results indicated that the PIN complex is dynamic, and NPA is not simply increasing the ability of pre-formed complexes to withstand detergent-mediated dissociation.

We next tested the hypothesis that PIN1 dimerization is necessary for NPA to inhibit PIN1 plants. Mab9B2, an anti-PIN1 monoclonal antibody, hinders the formation of NPA and quercetin-stabilized PIN1-PIN1 dimers *in vitro* (Fig 5A).

We expressed the corresponding Mab9B2 scFv fragments in plants under the control of the *PIN1* promoter (Fig EV4A–C). The resulting plants showed a resistance to NPA in polar auxin transport assays in stem sections and an insensitivity to IAA with respect to its effects on root length and lateral root density (Fig EV4D and E). The effect of NPA on three key physiological processes (lateral root formation, the gravitropic response and the angle of the dark-grown apical hook) was measured. All three processes are affected by NPA, but only during lateral root formation does PIN1 drive the

redistribution of auxin maxima (Benkova *et al*, 2003); it is PIN2 that plays a major role in gravitropism (Müller *et al*, 1998) and PINs 3, 4 and 7 in setting the angle of the apical hook (Zadnikova *et al*, 2010). If NPA-mediated PIN1 protein interactions are necessary for its ability to block PAT, we would expect to observe a specific insensitivity to NPA in *pPIN1::Mab9B2* plants during lateral root formation, but not in the gravitropic response or in the disruption of the apical hook formation. Lateral root formation is blocked at an early stage of development by NPA (Casimiro *et al*, 2001). Wild-type seedlings were therefore transferred, before lateral root emergence, at 4 days after germination (DAG) to medium containing NPA and grown for a further 5 days. This effectively inhibited lateral root emergence limiting densities at concentrations of NPA higher than 0.1 μ M to 0.3 lateral roots per cm (LR/cm) compared to a density of 1.1 LR/cm for untreated seedlings. Lateral root density did not decrease further at higher NPA concentrations, measuring 0.3 LR/cm at 5 μ M NPA. In contrast, lateral root density was independent of NPA concentration in *pPIN1::Mab9B2* plants (Fig 5B), remaining at 1 LR/cm at 5 μ M NPA (Fig 5C).

In contrast, no NPA resistance was measured in growth responses that are not considered to be primarily mediated by PIN1 (Fig 5D and E). For both apical hook formation and the gravitropic response, a significant resistance to NPA could be measured in *pPIN1::Mab9B2* plants (at between 0.5 and 1 μ M during gravitropism and between 0.1 and 1 μ M during apical hook formation). This phenomenon is consistent with a relatively rapid rootward PIN1-dependent flux of auxin when compared to NPA-blocked PIN2- and PIN3-dependent flux away from the root apical meristem. We hypothesize that the difference in effectiveness of NPA inhibition on different PIN proteins interfered with the establishment of auxin distribution during the gravitropic response and apical hook formation. In all three responses tested, growth was unaltered by Mab9B2 in the absence of NPA (Fig 5C–E). ScFv Mab9B2 does not therefore inhibit PIN function. A range of phenotypes was nevertheless observed in *pPIN1::Mab9B2* plants, ranging from an insensitivity to IAA in roots, smaller seeds and a higher proportion of withered seeds and rare morphological aberrations in leaf and stem architecture (Appendix Fig S4). These phenotypes are consistent with an altered capacity for endogenous PAT regulation (Blilou *et al*, 2005) or flavonoid metabolism (Doughty *et al*, 2014). We conclude that scFv Mab9B2 does not affect the ability of PIN1 to transport auxin from the cell but renders this transport insensitive to NPA whilst preventing PIN1 dimerization.

In order to map the scFv Mab9B2 epitope, a series of PIN1 fragments was expressed in *E. coli* and Western blot analyses with the intact antibody were performed. These experiments indicated that the epitope to which Mab9B2 binds lays in the central soluble domain of PIN1 between phenylalanine 280 and serine 320. In contrast, another monoclonal antibody, Mab10A7, bound to PIN1 between asparagine 232 and glycine 276. Unlike Mab10A7 (the antibody which was used to perform Western blot analysis in this study), in stripped and re-probed Western blots, Mab9B2 was only able to recognize the PIN1 monomer after BN-PAGE separation, suggesting dimerization specifically rendered its epitope inaccessible. Together, these results indicate that either an NPA-binding site or the dimerization interface is located in the region of the PIN1 polypeptide between glycine 276 and serine 320 (Fig EV5).

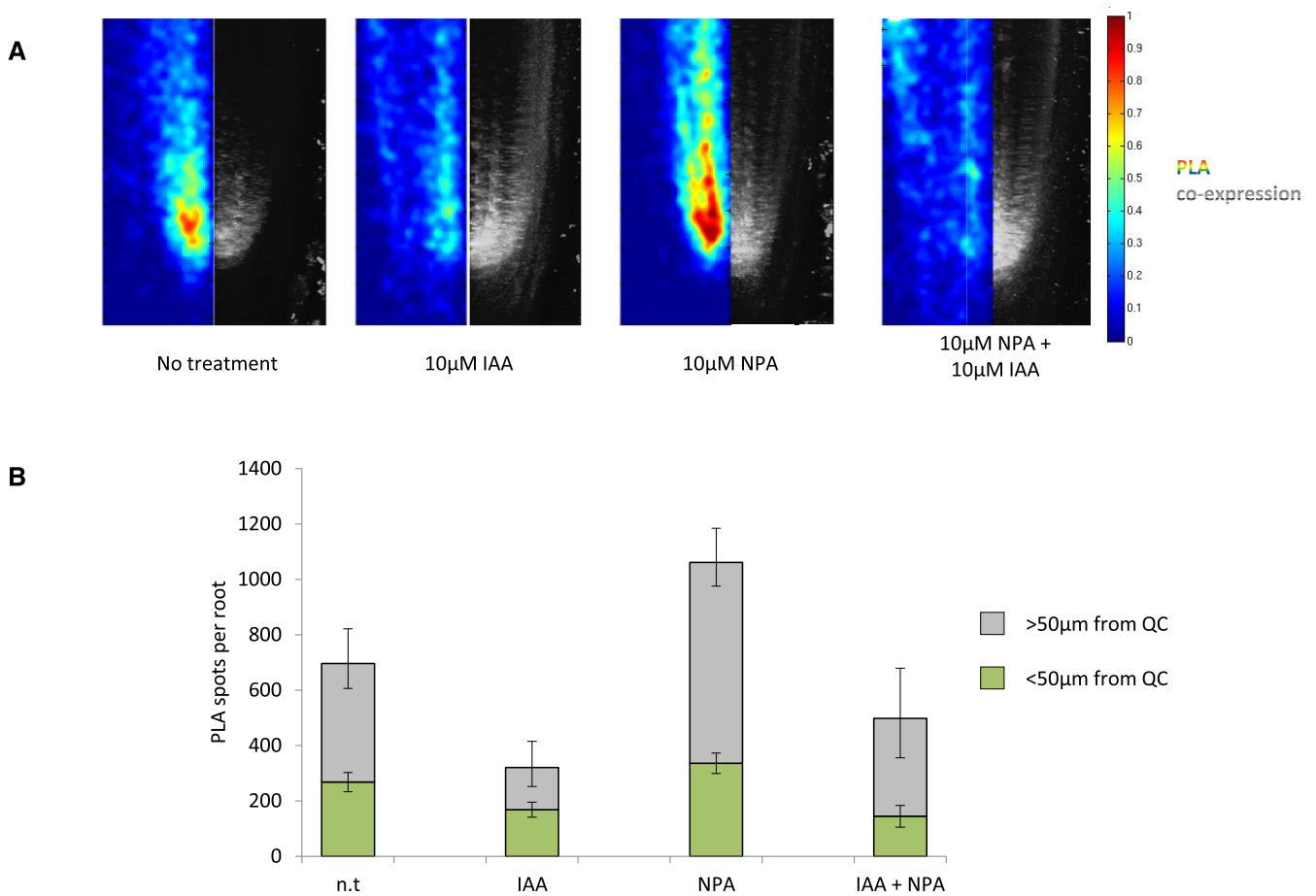


Figure 4. NPA induces PIN1-PIN4 interaction in vivo.

A Summed 2D projections of PLA interactions (left) and co-localization (right) ($n = 3$) between PIN1 and PIN4 laterally bisected 2D-projected heat map. Treatments as indicated.

B Quantification of positive PLA interactions. n.t. (no treatment) and 10 μ M NPA, $n = 4$; 10 μ M IAA and 10 μ M IAA + 10 μ M NPA, $n = 3$. Error bars indicate standard deviation.

Discussion

The regulation of auxin efflux coordinates many processes which are indispensable for the growth and development of plants and is therefore tightly regulated at many levels (Teale *et al.*, 2006; Adamowski & Friml, 2015). Members of two protein families: PINs (MFS proteins) and ABCB family proteins have, over the last twenty years, emerged as the most important efflux carriers. Furthermore, the transport activity of both has been shown to be regulated by the same synthetic flavonol analogue, NPA (Geisler *et al.*, 2005; Petrasek *et al.*, 2006). PIN1 and ABCB19 interact, forming a pairing which stabilizes PINs in specific nano-environments of the plasma membrane (Blakeslee *et al.*, 2007; Titapiwatanakun *et al.*, 2009). However, our data demonstrate that ABCB proteins do not form part of the smallest functional PIN complex (Fig 2). Instead, only a small fraction of purified PIN1, PIN2, PIN3, PIN4 or PIN7 proteins are associated with an ABCB-type auxin efflux protein (Fig EV1). This observation could be at least partially explained by the preferential solubilization of PINs under the

detergent conditions which we used; however, it cannot be used to refute the conclusion that PINs are able to transport auxin in heterologous cell assays (Fig 1; Zourelidou *et al.*, 2014), nor that the application of NPA to heterologously expressed membrane-bound PIN1 *in vitro* gives an ABCB-free stabilized core protein complex of the same size which is found in plant cells (Fig 3).

In this report, we show that PIN1-dependent cellular auxin efflux is inhibited by NPA. As NPA-sensitive ABCB19-dependent auxin efflux does not require PIN1, and as NPA blocks 25% of auxin efflux in protoplasts when used to test ABCB activity (Geisler *et al.*, 2005), we conclude that no active ABCB19 is present in the protoplasts isolated for this experiment and that ABCB19 is not necessary for PIN1 activity. It is, however, possible that PIN1-dependent auxin efflux is greatly enhanced by the presence of ABCB19 (or *vice versa*), and the fact that NPA can bind both ABCBs and PINs means that its ability to lower auxin efflux capacity may depend heavily on the environment of both proteins. Additionally, the relative functional consequences of interactions among ABCB proteins, the PIN core

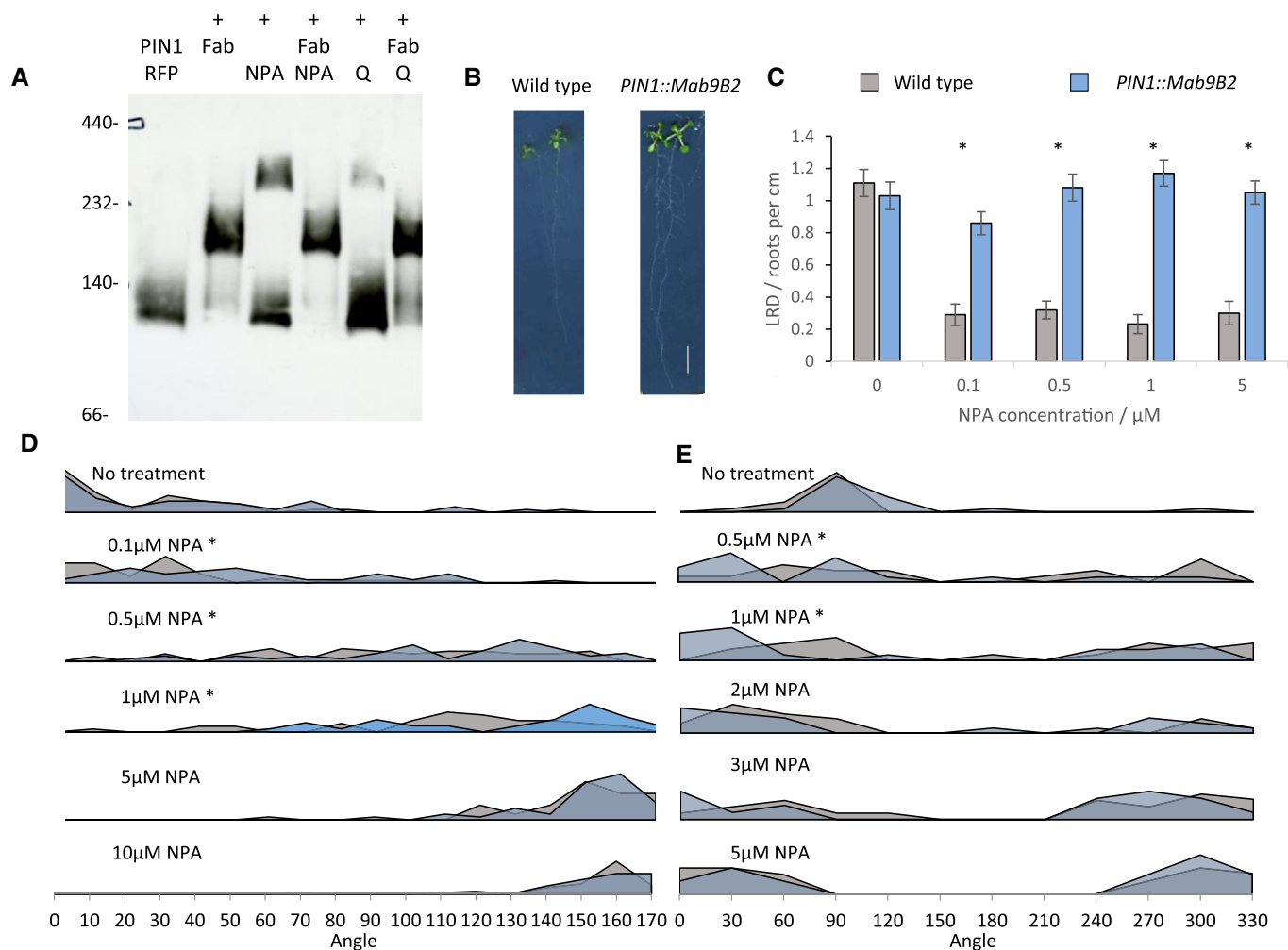


Figure 5. Inhibition of auxin transport by NPA requires PIN1 dimerization.

A Microsomes from HEK293 cells expressing PIN1-RFP were separated under native conditions in the presence of NPA or an anti-PIN1 Fab fragment. (1) PIN1-RFP, (2) PIN1-RFP + Fab, (3) PIN1-RFP + 10 μM NPA, (4) PIN1-RFP + Fab+10 μM NPA, (5) PIN1-RFP + 10 μM quercetin (Q) and (6) PIN1-RFP + Fab+10 μM quercetin (Q). Protein complexes were solubilized and separated under native conditions as described before. Western blots were performed with an anti-RFP monoclonal antibody.

B Fourteen-day-old Arabidopsis seedlings (wild type, brown; *pPIN1::Mab9B2*; blue) grown on AM containing 0.2 μM NPA. Scale bar = 1 cm.

C NPA-affected lateral root density of nine-day-old Arabidopsis seedlings expressing Mab9B2 scFv fragments (wild-type sample sizes were between 16 and 21 plants; Mab9B2 sample sizes were between 12 and 31 plants). Bars indicate standard error.

D NPA-affected apical hook angle in dark-grown three-day-old Arabidopsis seedlings expressing Mab9B2 scFv fragments. (wild-type sample sizes were between 38 and 50 plants; Mab9B2 sample sizes were between 33 and 45 plants).

E Gravitropic curvature in four-day-old Arabidopsis seedlings expressing Mab9B2 scFv fragments. (wild-type sample sizes were between 15 and 21 plants; Mab9B2 sample sizes were between 14 and 20 plants).

Data information: Asterisks indicate significant difference between genotypes ($P \leq 0.05$) after either a Student's *t*-test (C) or Kolmogorov–Smirnov (D, E) test.

complex and NPA may also affect the nano-environment of both proteins either directly or through its interaction of TWD1 with the actin cytoskeleton (Zhu *et al*, 2016).

Our results demonstrate that the immediate PIN1 protein environment is in a dynamic equilibrium between monomers and dimers which is susceptible to regulation by endogenous flavonols (Figs 3 and S2). A challenging interpretation of this observation is that a tight regulation of auxin efflux may be afforded by the majority of PIN1 molecules at any one time being localized to inactive protein complexes. Physically disrupting these PIN1-containing dimers with antibody fragments gives plants whose resistance to

NPA is confined to PIN1-mediated processes such as lateral root formation (Fig 5). This *in planta* test of the functional relevance of NPA-induced PIN1 dimerization relies on the demonstrated specificity of the anti-PIN1 antibody used (Blilou *et al*, 2005), but in future could be expanded to explore the physiological significance of endogenous PAT inhibition by using relevant crosses, such as *pin* loss-of-function controls and lines with altered flavonol metabolism. Whether flavonols such as quercetin and kaempferol are present in plants at concentrations significantly able to affect polar auxin transport rates has been ably discussed elsewhere (Jacobs & Rubery, 1988). However, here it should be noted that at least two enzymes

required for quercetin biosynthesis are polarly localized in growing roots, potentially leading to a much higher than anticipated concentration of quercetin here (Saslowky & Winkel-Shirley, 2001).

Oligomerization is a common phenomenon among major facilitator superfamily proteins, and its regulation is employed to control substrate transport rates (Hou *et al*, 2012). For example, dimerization of NRT1.1, a dual-affinity nitrate transporter in Arabidopsis, renders membranes less permeable to nitrate. Phosphorylation within the NRT1.1 protein–protein interface is inversely correlated with the rate of dimer formation (Sun *et al*, 2014; Sun & Zheng, 2015). A similar correlation is seen here with respect to PIN1: phosphorylation of the functionally important serine 290 both occurs within the putative protein–protein interface and increases membrane permeability to auxin (Huang *et al*, 2010). This raises the possibility that PIN phosphorylation status, at least in part, regulates auxin efflux rates either through affecting the ability of flavonols to interact with PIN1, or the propensity of PIN1 proteins to dimerize, or both. This hypothesis is supported by the observation that phenotypes caused by the over-expression of PINOID (an AGC kinase which directly phosphorylates PIN1) are abrogated by the application of NPA (Benjamins *et al*, 2001). Conversely, flavonols stabilize dimers and render membranes less permeable to auxin. It remains to be seen whether such post-translational fine-tuning of PIN1 regulates auxin transport rates by increasing the fraction of PIN1 present as active monomers.

Our analysis of the PIN1 protein complex indicates that under mild solubilization conditions, PIN1 is found in a protein complex of approximately 350 KDa. This complex is relatively easily disrupted by increasing the stringency of solubilization conditions (Fig 2). In the presence of progressively higher concentrations of NPA, disruption of the PIN1 dimer becomes increasingly difficult, with an NPA concentration of between 0.5 and 1 μ M being necessary for stabilization of a smaller 250 KDa complex. This concentration correlates well with those given for both the effective concentration for auxin transport inhibition and for the low-affinity microsomal-binding site (Michalke *et al*, 1992). We therefore conclude that NPA and flavonols interact with PIN1-containing protein complexes, simultaneously rendering them more stable and less able to mediate cellular auxin efflux.

The ability of NPA to directly inhibit PIN1-mediated auxin transport has, until now, been open to question, with experiments supporting (Yang & Murphy, 2009), ruling out (Kim *et al*, 2010) or leaving untested (Zourelidou *et al*, 2014) a role for NPA in diverse heterologous PIN1 assay systems. ABCB19, on the other hand, has garnered more widespread support as a direct target of NPA inhibition (Geisler *et al*, 2016). The question of whether PIN1 and ABCB19 act independently is also unresolved, with experiments either consistent (Mravec *et al*, 2008) or inconsistent (Bandyopadhyay *et al*, 2007; Rojas-Pierce *et al*, 2007) with this hypothesis. Our data support an interaction between PIN1 and ABCB19 in Arabidopsis (Blakeslee *et al*, 2007). However, the ratio of both proteins in PIN1-GFP affinity precipitates indicates that at any one time, the majority of PIN1 is not associated with ABCB19.

Flavonols either competitively or allosterically inhibit the function of a diverse range of proteins when applied to mammalian cells, including many enzyme families and some MFS transporters (Middleton *et al*, 2000; Kwon *et al*, 2007; Ojelabi *et al*, 2018). In plants, their function is also diverse, providing protection against

reactive oxygen species and high-energy light as well as non-competitively inhibiting polar auxin transport (Pollastri & Tattini, 2011). With respect to this third function, NPA may be considered as a synthetic analogue (Jacobs & Rubery, 1988). The NPA or flavonol-dependent stabilization of PINs expressed in HEK cells into dimers gives a molecular framework into which the similarity between the NPA-treated and *pin1* phenotypes can be reconciled: namely, that NPA application stabilizes PIN proteins into an inactive conformation, with endogenous flavonols performing this function *in vivo*. These observations are consistent with dynamic conformational changes within the PIN complex, the extent of which is dependent, at least in part, on local concentrations of flavonol and IAA.

Auxin counteracts the stabilizing effect of flavonols on the PIN1 core complex, potentially increasing the capacity for its own efflux. Regulation here is also likely to be complex, as the effect of both NPA and flavonols on PAT and PIN localization has been shown to vary with tissue and cell type (Rashotte *et al*, 2001; Kuhn *et al*, 2017). Although there exists a broad correlation between the ability of a flavonol to displace NPA from microsomal membranes and its capacity to inhibit PAT, notable exceptions exist. For example, morin binds tightly to plant microsomes, but is a poor PAT inhibitor (Jacobs & Rubery, 1988). Morin remains able to stabilize the PIN1 core complex relatively efficiently when compared to other flavonols, suggesting that complex stabilization and flavonol binding are more tightly linked than are dimer stability and auxin transport inhibition. It will therefore be informative further to explore the relationships between different flavonols and i) PIN-binding affinity, ii) induced changes to PIN subcellular localization and iii) the strength of PAT inhibition, to parse the mechanisms of endogenous PAT regulation.

Materials and Methods

Plant material

An overview of the different plant materials which were used for the following experiments is given in Table EV1. For auxin transport assays, protoplasts were prepared as previously described (Wend *et al*, 2013). In all other cases, *Arabidopsis thaliana* plants in the Columbia (Col-0) background were grown as follows: seeds were placed on plates containing Arabidopsis media (AM) $1/2$ MS and 1% agar with 1% sucrose and 2.5 mM 2-(N-morpholino)ethanesulfonic acid (MES) (pH 5.6). Plates were kept in darkness at 4°C for 16 h and then at 22°C under a 16-h light/8-h dark regime.

For affinity purification, roots of GFP-tagged *Arabidopsis thaliana* seedlings used the following lines: PIN1-GFP (Benkova *et al*, 2003), PIN2-GFP (Xu & Scheres, 2005), PIN3-GFP (Zadnikova *et al*, 2010) and ABCB19-GFP (Wu *et al*, 2007). Control purifications used the plasma membrane-localized LT16-GFP. Discrete lateral roots were induced by growing plants on AM containing 1.2% agar for 10 days before incubating in liquid medium containing 0.35 mg/l 2,4-dichlorophenoxyacetic acid for 16 h. After washing briefly with sterile H₂O, plants were then incubated with 0.1 mg/l 1-naphthaleneacetic acid for 3 days.

To obtain the *ProPIN4::PIN4-GFP* and *ProPIN7::PIN7-GFP* constructs, the full-length coding sequences of AtPIN4 and AtPIN7, inclusive of their native promoters, introns and 3'UTRs, were amplified by PCR from genomic DNA (*Arabidopsis* cv Columbia) with the

primer pairs: 5'-TCTCTCAGATGTGTCTAAAG-3' (containing the EcoRI site) and 5'-GTTCCGTTGTTGCCGCCG-3' (containing the StuI site) for the first fragment of PIN4; 5'-TATGCCGCCGA CAAGTG-3' (containing the SpeI site) and 5'-ATGTAAGCA TAATGGTTCATG-3' (containing the Sall site) for the second fragment of PIN4; 5'-CAAGAGGGATAAACCGACGC-3' (containing the EcoRI site) and 5'- CCTTACCCTCTCCGACTCTTC-3' (containing the KpnI site) for the first fragment of PIN7; 5'-AAGTGCCTAACG-GACTAC-3' (containing the BglII site) and 5'-CGCCTAATCGTAAC-TAAGAGG-3' (containing the Sall site) for the second fragment of PIN7. The PIN4 and PIN7 genomic fragments were translationally fused to the GFP coding sequence in frame at positions 446 and 418 from the start codon, respectively, by cloning the first and second PCR-amplified genomic fragments upstream and downstream of the GFP coding sequence in the vector pGJ-317 (Ottenschlager *et al*, 2003). The obtained *ProPIN::PIN-GFP* constructs were sequence-verified, excised from the pGJ-317 vector and subsequently cloned into the pGJ-Bar binary vector by EcoRI-Sall restriction sites. Plant transformation and selection were carried out as described previously (Molendijk *et al*, 2008).

Binary interactions were verified after *Agrobacterium tumefaciens*-mediated transient protein expression in leaves of *Nicotiana benthamiana* as previously described (Sparkes *et al*, 2006). Genes were cloned, using the GATEWAY system (Thermo Fisher), into pB2GW7 or pEARLEY vectors (Earley *et al*, 2006).

For blue-native PAGE separations, microsomal preparations were prepared from MM2d Arabidopsis cell suspension cultures maintained in MS medium with 3% (w/v) sucrose, 0.5 mg/l NAA and 0.05 mg/l kinetin, pH 5.8, in continuous darkness at 130 rpm at 27°C and subcultured every seven days (Menges *et al*, 2002).

cDNAs encoding anti-PIN1 scFv fragments were constructed after reverse transcription of mRNA encoding short-chain antibody fragments from hybridoma cell cultures was amplified using the following primers: heavy chain variable domain MHV.B4 5'-CAGGTTACT CTGAAAGAGTC-3'; kappa chain variable domain MKV.B4 5'-GACATTGTGCTGACCCAATCT-3'. Fragments were then joined using overlap extension PCR with the following primers: Linker rev (MHC.F) 5'-CTCGAGGTCGACCTGCAGCTGCACCTGTTGGGGGTG TCGTTTTG-3'; MKV.B10 Linker 5'-GGTCGACCTCGAGATCAAA CGGACGCGTAGACATTCTGATGACCCA-3'. cDNAs encoding scFvs were then transformed into *Arabidopsis thaliana* ecotype Columbia (Col0) under control of the *PIN1* promoter (Benkova *et al*, 2003; pB2GW7; Mab9B2_attb1: 5'-GGGGACAAGTTTGTACAAAAAAGCAG GCTTTATGcaGgTTaCTCTGAAAGAGTCTG-3'; Common_attb2_rev: 5'-GGGGACCACTTTGTACAAAGAAAGCTGGGTTGATACAGTTGGT GCAGCATC-3'). Homozygous plants were used for all experiments. RT-PCR and Western blotting used homogenized four-day-old seedlings. For Western blots, HRP-conjugated protein L (GenScript) was used at 1:5,000 according to the manufacturer's instructions. The ability of NPA to inhibit polar auxin transport was measured in an assay based on a previously published protocol (Lewis & Muday, 2009), with the following modifications. Basal stem segments of 2.5 cm were used for the assay, incubated in the dark at room temperature for 16 h in 20 μ l 3 H-IAA 10 nCi in 5% MES pH 5.5. Tritium was measured by scintillation counting in 1-cm stem segments taken 0.5 cm from the basal end. Polar transport was calculated by subtracting tritium dpm in identically treated segments, but incubated with their basal ends instead of their apical ends in the 3 H-IAA solution.

Chemicals

All chemicals were of analytical grade and purchased from commercial sources. For those chemicals with poor solubility in water, 100 mM (or 1,000 \times) stocks were prepared in either DMSO or 1 M KOH. Detergent mixtures ComplexioLyte 27 and ComplexioLyte 47 were kindly provided by Logopharm GmbH.

Auxin efflux assay

A protoplast-based auxin efflux assay was performed exactly as previously described (Wend *et al*, 2013). 10 μ M NPA was added to protoplast isolated from Arabidopsis mesophyll cells 5 min before the IAA, a 30-min incubation was then performed before protoplasts were recovered, and luminescence was measured in triplicate for each substrate and sample for 1 s each.

Affinity purification

One hundred and twenty milligram of roots was harvested for each purification and homogenized in 1.4 ml ice-cold Tris-HCl saline buffer (150 mM NaCl, 50 mM Tris-HCl pH 8) containing complete protease inhibitors (Roche) in a glass potter on ice before centrifugation for 30 min at 150,000 g. The membrane pellet was resuspended in 540 μ l ml Tris-HCl saline buffer and 100 μ l detergent stock solution and solubilized for one hour at 7°C with rotation. Samples were then once more centrifuged for 30 min at 150,000 g. Affinity purification used 50 μ l μ MACS-anti-GFP or streptavidin beads (Miltenyi Biotec). Samples were incubated with beads for 90 min at 7°C with rotation before the mixture was applied to a column pre-equilibrated with Tris-HCl saline buffer containing 1% Triton X-100 (w/v). Columns were then washed six times with 200 μ l homogenization buffer containing 1:10 diluted ComplexioLyte 47 (Fig 2C) 0.1% DDM (w/v, Fig EV1B) then 1 \times with 100 μ l wash buffer 2 (Miltenyi Biotec). Proteins were eluted with 80 μ l Laemmli buffer.

Mass spectrometry

Samples for LC-MS/MS analysis were prepared and measured as previously described (Schwenk *et al*, 2014). Briefly, proteins eluted from APs were shortly run on SDS-PAGE gels and silver-stained, and lanes were cut into two sections (> and <50 kDa MW). In-gel digestion with sequencing-grade modified trypsin (Promega, Mannheim, Germany) was carried out following a standard procedure (Pandey *et al*, 2000). Extracted peptides were vacuum-dried and redissolved in 0.5% trifluoroacetic acid, loaded onto a trap column (C18 PepMap 100, 5- μ m particles; Thermo Scientific) with 0.05% trifluoroacetic acid (20 μ l/min for 5 min) and separated by reversed-phase chromatography via a 10-cm C18 column (PicoTip™ Emitter, 75 μ m, tip: 8 μ m; New Objective, self-packed with ReproSil-Pur 120 ODS-3, 3 μ m, Dr. Maisch HPLC; flow rate: 300 nl/min) using an UltiMate 3000 RSLCnano HPLC System (Thermo Scientific). Aqueous organic elution gradient (eluent "A": 0.5% acetic acid; eluent "B": 0.5% acetic acid in 80% acetonitrile): "A"/"B" gradient: 5 min 3% B, 60 min from 3% B to 30% B, 15 min from 30% B to 99% B, 5 min 99% B, 5 min from 99% B to 3% B, and 15 min 3% B). Sensitive and high-resolution MS analyses were carried out on an Orbitrap Elite mass spectrometer equipped with a

Nanospray Flex Ion Source (both Thermo Scientific). Precursor signals (LC-MS) were acquired with a target value of 1,000,000 and a nominal resolution of 240,000 (FWHM) at m/z 400, scan range: 370 to 1,700 m/z . Up to ten data-dependent CID fragment ion spectra (isolation width of 1.0 m/z with wideband activation) per scan cycle were allowed in the ion trap with a target value of 10,000 (maximum injection time of 200 ms for complex mixtures and 400 ms for gel bands) with dynamic exclusion (exclusion duration: 30 s; exclusion mass width: ± 20 ppm), preview mode for FTMS master scans, charge state screening, monoisotopic precursor selection and charge state rejection enabled.

LC-MS/MS data were extracted using “msconvert.exe” (part of ProteoWizard; <http://proteowizard.sourceforge.net/>, version 3.0.6906). Peak lists were searched against a combined Arabidopsis database using Mascot 2.6.0 (Matrix Science, UK). Preliminary searches with high peptide mass tolerance (± 50 ppm) were used for linear shift mass recalibration by a home-written script. Final searches were carried out with ± 5 ppm and ± 0.8 Da for precursor m/z and fragment ion spectra, respectively. One missed trypsin cleavage and common variable modifications including S/T/Y phosphorylation were accepted for peptide identification. Significance threshold was set to $P < 0.05$. Proteins identified by only one specific MS/MS spectrum or representing exogenous contaminations such as trypsin, keratins or immunoglobulins were eliminated.

Label-free quantification of proteins was based on peak volumes (PVs = peptide m/z signal intensities integrated over time) of peptide features extracted with MaxQuant (<http://www.coxdocs.org/> 48, version 1.4) with integrated effective mass calibration. Features were then aligned between different LC-MS/MS runs and assigned directly or indirectly to identified peptides with retention time tolerance ± 1 min and mass tolerance ± 1.5 ppm using an in-house developed software tool. Resulting peptide PV data were used for estimation of absolute abundance (abundancenorm values, calculated as the sum of all protein-specific peptide PVs divided by the number of amino acids from the respective protein sequence accessible to MS analysis under the conditions used) and for determination of (co)purification specificity (protein ratios, rPV) using the TopCorr method (median of at least 2–6 individual peptide PV ratios of the best correlating protein-specific peptides (Bildl *et al*, 2012)). Proteins were considered specifically co-purified when their rPV (from root tissue expressing the respective GFT-tagged target versus root tissue expressing a GFP control (GFP-LTi6)) exceeded a critical threshold (between 10 and 20) determined from respective rPV histograms. Primary results were further scrutinized by manual inspection of their PV values and their consistency in different APs.

Heterologous expression of PIN1

Sequences encoding either PIN1 or PIN1-RFP were cloned into pBK and transformed into HEK293T cells.

Mutagenesis of the *PIN1* gene in the pBK vector was performed according to QuikChange Site-Directed Mutagenesis Kit (Agilent Technologies). A TCT to GAA codon change was introduced to obtain the S252/253E and S261E mutations. The primer sequences used for SDM were as follows: S252/253E forward AACCCAACGCCACGTGGCGAAGAATTTAATCATACTGATTTTTAC, S252/253E reverse GTAAAAATCAGTATGATTAAATTTCTTCGCCACGTGGCGTT

GGGTT, S261E forward TTTAATCATACTGATTTTTACGAAATGATGGCTTCTGGTGGTGGT, S261E reverse ACCACCACCAGAAGC-CATCATTTTCGTAAAAATCAGTATGATTTAA.

Cells were grown at 37°C in vented cell culture flasks under 5% CO₂. Briefly, 10–30,000 cells were grown in complete growth medium per 10-cm dish and incubated overnight. At 50–80% confluence before transfection, 3 μ l GeneJuice Transfection Reagent (Novagen) per μ g DNA was added to 800 μ l serum-free medium (DMEM) and added dropwise to cells in complete growth medium. Cells were then incubated for between 24 and 72 h. Cells were then washed twice with 1 \times PBS and harvested at 3,000 g before resuspension in 3 ml 10 mM Tris-HCl pH 7.5, 0.5 mM MgCl₂. Cells were incubated on ice for 10 min before homogenization with a Dounce homogenizer. 3 ml of 10 mM Tris-HCl pH 7.5, 0.5 M sucrose and 0.3M KCl was then added. Lysate was cleared by centrifugation at 4,000 g for 10 min. Supernatants were then diluted with 30 ml of 5 mM Tris-HCl pH 7.5, 0.25 M sucrose and 0.15 M KCl and centrifuged at 100,000 g for one hour. The resulting microsomal pellets were resuspended in 1 \times PBS buffer.

1D-BN-PAGE analysis

1D-BN-PAGE followed a previously published protocol (Wittig *et al*, 2006). Microsomes were prepared after suspension cells were homogenized using a pressure lysis unit (Constant Systems Ltd) in 330 mM sucrose, 50 mM potassium phosphate buffer and 10 mM sodium fluoride and containing a complete protease inhibitor cocktail (Roche). Samples were cleared by centrifugation at 8,000 g for 15 min before membranes were harvested at 100,000 g for one hour and resuspended in homogenization buffer.

Briefly, for each lane, plant microsomes containing 10 μ g protein were solubilized in a final volume of 100 μ l on ice for one hour with 50% (v/v) ComplexioLyte 27. 6.3 μ l 5% Coomassie blue G250 was added and incubated for another 15 min. Ten microliter of 50% glycerol was added and the sample mixed well before half the sample volume was loaded. 5–12% gradient gels were run at 150 volts with cathode buffer containing 0.02% Coomassie blue until a third of the gel was run, after which Coomassie blue in the cathode buffer was reduced to 0.002% (w/v) (overnight at 7°C). Transfer of 1D-BN-PAGE-separated proteins onto PVDF membrane was performed in 50 mM tricine and 7.5 mM imidazole at pH 7.0 for 16 h at 40V. Membranes were then washed in 25% methanol and 10% (v/v) acetic acid before washing twice in PBS-T containing 0.1% (v/v) Tween-20. PVDF membranes were blocked in 4% (w/v) milk powder in PBS-T for one hour. Hybridoma supernatants containing monoclonal primary antibodies were used at 1:50 in 4% milk powder in PBS-T for one hour, and HRP-conjugated secondary antibodies were used at a 1:3,000 dilution, also for 1 h. Bound antibodies were visualized with SuperSignal West Pico Chemiluminescent Substrate (Invitrogen) and exposed to X-ray film (Amersham Hyperfilm ECL), or visualized with a CCD camera (Peqlab). Densitometry of digitally taken images was performed in triplicate with ImageJ.

2D-BN-PAGE analysis

Non-denaturing 1–14% (v/v acrylamide) gradient gels (14 \times 11 cm, 1.5 mm spacer) were manually cast (gel buffer 0.75 M aminocaproic acid, 50 mM BisTris, pH 7.0 and 0.1% CL47 detergent). 0.5 mg of Arabidopsis root membranes was solubilized in 0.5 ml of

detergent buffer (CL47 and CL27, protein–detergent ratio of 1:10, with 1 mM EDTA/EGTA and protease inhibitors added) for 20 min on ice and cleared by ultracentrifugation (12 min at 100,000 g). The supernatant was supplemented with 10% sucrose and directly loaded onto the gel. After the run, gel lanes were excised, equilibrated for 2 × 10 min in 2× Laemmli buffer and loaded onto 10% SDS–PAGE gels for second dimension separation followed by Western blotting onto PVDF membranes. Western blot detection was carried out using mouse monoclonal anti-PIN1 (Blilou *et al*, 2005) and HRP-conjugated secondary ABs (Santa Cruz Biotechnology) and ECL Prime (Sigma-Aldrich). Protein complexes visible in total protein stains of the respective Western blot membranes (SYPRO Ruby Protein Blot Stain, Bio-Rad) were used as markers for the apparent molecular mass of complexes.

Whole-mount proximity ligation assay and immunolocalization

Five-day-old wild-type seedlings were fixed and permeabilized as previously described (Pasternak *et al*, 2015). Primary antibody incubation (1:40 for anti-PIN1 mouse [clone 7E7] and 1:200 for anti-PIN4 rabbit [serum 9105]) was for two hours at room temperature followed by incubation for 10 h at 4°C. Roots were then washed with MTSB and incubated at 37°C for four hours either with Alexa-conjugated anti-mouse 488 and anti-rabbit 555 for co-localization or anti-mouse plus and anti-rabbit minus for PLA (Duolink). PLA samples were then washed with MTSB buffer and treated for three subsequent hours with ligase solution at 37°C. Plants were then washed with buffer B (2 × 5 min) and treated for 4–5 h in polymerase solution containing fluorescent nucleotides at 37°C as described by the manufacturer (Sigma-Aldrich). Samples were then washed with buffer B (2 × 5 min) and then with 1% buffer B for 5 min before mounting on microscopic slides in DAPI Gold reagent. For PIN1-PIN4 co-localization, Alexa-conjugated secondary antibodies (anti-mouse 488 and anti-rabbit 680) were added to buffer B and incubated for 30 min before washing with buffer B.

Microscopy

PLA-stained samples were recorded using a confocal laser scanning microscope (ZEISS LSM 510 Duo-Live) with a C-Apochromat 40×/1.2 W corr. objective. For the DAPI excitation, a 405-nm diode laser was used and emission detected with a long-pass filter (LP 420); PLA excitation was at 561 nm and emission detected with a band-pass filter (LP 650). Serial optical sections were reconstituted into 3D image stacks to a depth of 120 μm with in-plane (x-y) voxel extents of 0.15-μm and 0.9-μm section spacing (z).

Image processing and analysis

Images were converted to hdf5 format. Nuclei were annotated automatically, and the dQC was manually corrected using the iRoCS Toolbox and the coordinate system automatically attached to the root recording (Schmidt *et al*, 2014).

Data availability

All reagents and materials are available upon request from the corresponding author (william.teale@biologie.uni-freiburg.de). Proteomic

data sets have been deposited at the Proteomics Identification Database—EMBL-EBI (PRIDE) (<https://www.ebi.ac.uk/pride>) with the data set identifier PXD021543.

Expanded View for this article is available online.

Acknowledgements

The authors acknowledge Young Jun Cho and Zuzanna Kazimierczak for their technical assistance. This work was supported by Bundesministerium für Bildung und Forschung (BMBF SYSBRA, SYSTEC, Microsystems), the Excellence Initiative of the German Federal and State Governments (EXC 294) and the German Research Foundation (DFG SFB746 and INST 39/839,840,841). C.D.B. acknowledges support from Deutsches Zentrum für Luft und Raumfahrt (DLR 50WB1022). Open access funding enabled and organized by Projekt DEAL.

Author contributions

W.T. and K.P. conceived the study. W.T. wrote the manuscript. T.P., C.D.B., A.D., K.K., U.S., M.Sch., M.Sh., L.P. and F.L. planned and performed experiments and analysed the data. B.R., J.V.S., T.F., X.L. and A.P. produced and were responsible for resources. W.B. and U.S. planned and performed proteomic measurements and analysed the data. W.T., U.S. and K.P. supervised the study. U.S. and K.P. acquired the funding.

Conflict of interest

The authors declare that they have no conflict of interest.

References

- Adamowski M, Friml J (2015) PIN-dependent auxin transport: action, regulation, and evolution. *Plant Cell* 27: 20–32
- Bailly A, Sovero V, Vincenzetti V, Santelia D, Bartnik D, Koenig BW, Mancuso S, Martinoia E, Geisler M (2008) Modulation of P-glycoproteins by auxin transport inhibitors is mediated by interaction with immunophilins. *J Biol Chem* 283: 21817–21826
- Bandyopadhyay A, Blakeslee JJ, Lee OR, Mravec J, Sauer M, Titapiwatanakun B, Makam SN, Bouchard R, Geisler M, Martinoia E, *et al* (2007) Interactions of PIN and PGP auxin transport mechanisms. *Biochem Soc Trans* 35: 137–141
- Benjamins R, Quint A, Weijers D, Hooykaas P, Offringa R (2001) The PINOID protein kinase regulates organ development in Arabidopsis by enhancing polar auxin transport. *Development* 128: 4057–4067
- Benkova E, Michniewicz M, Sauer M, Teichmann T, Seifertova D, Jurgens G, Friml J (2003) Local, efflux-dependent auxin gradients as a common module for plant organ formation. *Cell* 115: 591–602
- Bildl W, Haupt A, Muller CS, Biniossek ML, Thumfart JO, Huber B, Fakler B, Schulte U (2012) Extending the dynamic range of label-free mass spectrometric quantification of affinity purifications. *Mol Cell Proteomics* 11: M111.007955
- Blakeslee JJ, Bandyopadhyay A, Lee OR, Mravec J, Titapiwatanakun B, Sauer M, Makam SN, Cheng Y, Bouchard R, Adamec J *et al* (2007) Interactions among PIN-FORMED and P-glycoprotein auxin transporters in Arabidopsis. *Plant Cell* 19: 131–147
- Blilou I, Xu J, Wildwater M, Willemsen V, Paponov I, Friml J, Heidstra R, Aida M, Palme K, Scheres B (2005) The PIN auxin efflux facilitator network controls growth and patterning in Arabidopsis roots. *Nature* 433: 39–44
- Brauchle M, Hansen S, Caussinus E, Lenard A, Ochoa-Espinosa A, Scholz O, Sprecher SG, Pluckthun A, Affolter M (2014) Protein interference

- applications in cellular and developmental biology using DARPins that recognize GFP and mCherry. *Biol Open* 3: 1252–1261
- Brown DE, Rashotte AM, Murphy AS, Normanly J, Tague BW, Peer WA, Taiz L, Muday GK (2001) Flavonoids act as negative regulators of auxin transport in vivo in *Arabidopsis*. *Plant Physiol* 126: 524–535
- Buer CS, Kordbacheh F, Truong TT, Hocart CH, Djordjevic MA (2013) Alteration of flavonoid accumulation patterns in transparent testa mutants disturbs auxin transport, gravity responses, and imparts long-term effects on root and shoot architecture. *Planta* 238: 171–189
- Casimiro I, Marchant A, Bhalerao RP, Beeckman T, Dhooge S, Swarup R, Graham N, Inze D, Sandberg G, Casero PJ et al (2001) Auxin transport promotes *Arabidopsis* lateral root initiation. *Plant Cell* 13: 843–852
- Dreier B, Mikheeva G, Belousova N, Parizek P, Boczek E, Jelesarov I, Forrer P, Pluckthun A, Krasnykh V (2011) Her2-specific multivalent adapters confer designed tropism to adenovirus for gene targeting. *J Mol Biol* 405: 410–426
- Doughty J, Aljabri M, Scott RJ (2014) Flavonoids and the regulation of seed size in *Arabidopsis*. *Biochem Soc Trans* 42: 364–369
- Earley KW, Haag JR, Pontes O, Opper K, Juehne T, Song K, Pikaard CS (2006) Gateway-compatible vectors for plant functional genomics and proteomics. *Plant J* 45: 616–629
- Friml J, Yang X, Michniewicz M, Weijers D, Quint A, Tietz O, Benjamins R, Ouwerkerk PB, Ljung K, Sandberg G et al (2004) A PINOID-dependent binary switch in apical-basal PIN polar targeting directs auxin efflux. *Science* 306: 862–865
- Geisler M, Bailly A, Ivanchenko M (2016) Master and servant: Regulation of auxin transporters by FKBP and cyclophilins. *Plant Sci* 245: 1–10
- Geisler M, Blakeslee JJ, Bouchard R, Lee OR, Vincenzetti V, Bandyopadhyay A, Titapiwatanakun B, Peer WA, Bailly A, Richards EL et al (2005) Cellular efflux of auxin catalyzed by the *Arabidopsis* MDR/PGP transporter AtPGP1. *Plant J* 44: 179–194
- Hertel R, Leopold AC (1962) Auxintransport und Schwerkraft. *Die Naturwissenschaften* 49: 377–378
- Hertel R, Lomax TL, Briggs WR (1983) Auxin transport in membrane-vesicles from *Cucurbita pepo* L. *Planta* 157: 193–201
- Hou Z, Kugel Desmoulin S, Etryre E, Olive M, Hsiung B, Cherian C, Wloszczynski PA, Moin K, Matherly LH (2012) Identification and functional impact of homo-oligomers of the human proton-coupled folate transporter. *J Biol Chem* 287: 4982–4995
- Huang F, Zago MK, Abas L, van Marion A, Galvan-Ampudia CS, Offringa R (2010) Phosphorylation of conserved PIN motifs directs *Arabidopsis* PIN1 polarity and auxin transport. *Plant Cell* 22: 1129–1142
- Jacobs M, Rubery PH (1988) Naturally-occurring auxin transport regulators. *Science* 241: 346–349
- Jenness MK, Carraro N, Pritchard CA, Murphy AS (2019) The *Arabidopsis* ATP-BINDING CASSETTE transporter ABCB21 regulates auxin levels in cotyledons, the root pericycle, and leaves. *Front Plant Sci* 10: 806
- Katekar GF, Geissler AE (1980) Auxin transport inhibitors. 4. Evidence of a common-mode of action for a proposed class of auxin transport inhibitors – the phytohormones. *Plant Physiol* 66: 1190–1195
- Kim J-Y, Henrichs S, Bailly A, Vincenzetti V, Sovero V, Mancuso S, Pollmann S, Kim D, Geisler M, Nam H-G (2010) Identification of an ABCB/P-glycoprotein-specific inhibitor of auxin transport by chemical genomics. *J Biol Chem* 285: 23307–23315
- Kuhn BM, Nodzynski T, Errafi S, Bucher R, Gupta S, Aryal B, Dobrev P, Bigler L, Geisler M, Zazimalova E, et al (2017) Flavonol-induced changes in PIN2 polarity and auxin transport in the *Arabidopsis thaliana rol1-2* mutant require phosphatase activity. *Sci Rep* 7: 41906
- Kwon O, Eck P, Chen S, Corpe CP, Lee JH, Kruhlak M, Levine M (2007) Inhibition of the intestinal glucose transporter GLUT2 by flavonoids. *FASEB J* 21: 366–377
- Lewis DR, Muday GK (2009) Measurement of Auxin Transport in *Arabidopsis thaliana*. *Nat Protoc* 4: 437–451
- Menges M, Hennig L, Gruissem W, Murray JA (2002) Cell cycle-regulated gene expression in *Arabidopsis*. *J Biol Chem* 277: 41987–42002
- Michalke W, Katekar GF, Geissler AE (1992) Phytohormone-binding sites and auxin transport in *Cucurbita-pepo* – evidence for 2 recognition sites. *Planta* 187: 254–260
- Michniewicz M, Zago MK, Abas L, Weijers D, Schweighofer A, Meskiene I, Heisler MG, Ohno C, Zhang J, Huang F et al (2007) Antagonistic regulation of PIN phosphorylation by PP2A and PINOID directs auxin flux. *Cell* 130: 1044–1056
- Middleton Jr E, Kandaswami C, Theoharides TC (2000) The effects of plant flavonoids on mammalian cells: implications for inflammation, heart disease, and cancer. *Pharmacol Rev* 52: 673–751
- Molendijk AJ, Ruperti B, Singh MK, Dovzhenko A, Ditengou FA, Milia M, Westphal L, Rosahl S, Soellick TR, Uhrig J et al (2008) A cysteine-rich receptor-like kinase NCRK and a pathogen-induced protein kinase RBK1 are Rop GTPase interactors. *Plant J* 53: 909–923
- Morgan DG, Soding H (1958) Über die Wirkungsweise von Phthalsäuremono-alpha-Naphthylamid (PNA) auf das Wachstum der Haferkoleoptile. *Planta* 52: 235–249
- Mravec J, Kubes M, Bielach A, Gaykova V, Petrasek J, Skupa P, Chand S, Benkova E, Zazimalova E, Friml J (2008) Interaction of PIN and PGP transport mechanisms in auxin distribution-dependent development. *Development* 135: 3345–3354
- Müller A, Guan C, Galweiler L, Tanzler P, Huijser P, Marchant A, Parry G, Bennett M, Wisman E, Palme K (1998) AtPIN2 defines a locus of *Arabidopsis* for root gravitropism control. *EMBO J* 17: 6903–6911
- Noh B, Murphy AS, Spalding EP (2001) Multidrug resistance-like genes of *Arabidopsis* required for auxin transport and auxin-mediated development. *Plant Cell* 13: 2441–2454
- Ojelabi OA, Lloyd KP, De Zutter JK, Carruthers A (2018) Red wine and green tea flavonoids are cis-allosteric activators and competitive inhibitors of glucose transporter 1 (GLUT1)-mediated sugar uptake. *J Biol Chem* 293: 19823–19834
- Okada K, Ueda J, Komaki MK, Bell CJ, Shimura Y (1991) Requirement of the auxin polar transport-system in early stages of *Arabidopsis* floral bud formation. *Plant Cell* 3: 677–684
- Ottenschlager I, Wolff P, Wolverton C, Bhalerao RP, Sandberg G, Ishikawa H, Evans M, Palme K (2003) Gravity-regulated differential auxin transport from columella to lateral root cap cells. *Proc Natl Acad Sci USA* 100: 2987–2991
- Paciorek T, Zazimalova E, Ruthardt N, Petrasek J, Stierhof YD, Kleine-Vehn J, Morris DA, Emans N, Jurgens G, Geldner N, et al (2005) Auxin inhibits endocytosis and promotes its own efflux from cells. *Nature* 435: 1251–1256
- Paponov IA, Teale WD, Trebar M, Blilou I, Palme K (2005) The PIN auxin efflux facilitators: evolutionary and functional perspectives. *Trends Plant Sci* 10: 170–177
- Pandey A, Andersen JS, Mann M (2000) Use of mass spectrometry to study signaling pathways. *Sci Signal* 2000: pl1.
- Pasternak T, Teale W, Falk T, Ruperti B, Palme K (2018) A PLA-iRoCS pipeline for the localization of protein-protein interactions in situ. *Methods Mol Biol* 1787: 161–170

- Pasternak T, Tietz O, Rapp K, Begheldo M, Nitschke R, Ruperti B, Palme K (2015) Protocol: an improved and universal procedure for whole-mount immunolocalization in plants. *Plant Methods* 11: 50
- Peer WA, Brown DE, Tague BW, Muday GK, Taiz L, Murphy AS (2001) Flavonoid accumulation patterns of transparent testa mutants of *Arabidopsis*. *Plant Physiol* 126: 536–548
- Petrasek J, Mravec J, Bouchard R, Blakeslee JJ, Abas M, Seifertova D, Wisniewska J, Tadele Z, Kubes M, Covanova M et al (2006) PIN proteins perform a rate-limiting function in cellular auxin efflux. *Science* 312: 914–918
- Pollastri S, Tattini M (2011) Flavonols: old compounds for old roles. *Ann Bot* 108: 1225–1233
- Rashotte AM, DeLong A, Muday GK (2001) Genetic and chemical reductions in protein phosphatase activity alter auxin transport, gravity response, and lateral root growth. *Plant Cell* 13: 1683–1697
- Reinhardt D, Mandel T, Kuhlemeier C (2000) Auxin regulates the initiation and radial position of plant lateral organs. *Plant Cell* 12: 507–518
- Rojas-Pierce M, Titapiwatanakun B, Sohn EJ, Fang F, Larive CK, Blakeslee J, Cheng Y, Cutler SR, Peer WA, Murphy AS et al (2007) *Arabidopsis* P-glycoprotein19 participates in the inhibition of gravitropism by gravacin. *Chem Biol* 14: 1366–1376
- Rubery PH (1990) Phytotropins – receptors and endogenous ligands. *Symp Soc Exp Biol* 44: 119–146.
- Saslosky D, Winkel-Shirley B (2001) Localization of flavonoid enzymes in *Arabidopsis* roots. *Plant J* 27: 37–48
- Schmidt T, Pasternak T, Liu K, Blein T, Aubry-Hivet D, Dovzhenko A, Duerr J, Teale W, Ditengou FA, Burkhardt H et al (2014) The iRoCS Toolbox – 3D analysis of the plant root apical meristem at cellular resolution. *Plant J* 77: 806–814
- Schwenk J, Baehrens D, Haupt A, Bildl W, Boudkkazi S, Roeper J, Fakler B, Schulte U (2014) Regional diversity and developmental dynamics of the AMPA-receptor proteome in the mammalian brain. *Neuron* 84: 41–54
- Sparkes IA, Runions J, Kearns A, Hawes C (2006) Rapid, transient expression of fluorescent fusion proteins in tobacco plants and generation of stably transformed plants. *Nat Protoc* 1: 2019–2025
- Sun J, Zheng N (2015) Molecular Mechanism Underlying the Plant NRT1.1 Dual-Affinity Nitrate Transporter. *Front Physiol* 6: 386
- Sun J, Bankston JR, Payandeh J, Hinds TR, Zagotta WN, Zheng N (2014) Crystal structure of the plant dual-affinity nitrate transporter NRT1.1. *Nature* 507: 73–77
- Teale WD, Paponov IA, Palme K (2006) Auxin in action: signalling, transport and the control of plant growth and development. *Nat Rev Mol Cell Biol* 7: 847–859
- Titapiwatanakun B, Blakeslee JJ, Bandyopadhyay A, Yang H, Mravec J, Sauer M, Cheng Y, Adamec J, Nagashima A, Geisler M et al (2009) ABCB19/PGP19 stabilises PIN1 in membrane microdomains in *Arabidopsis*. *Plant J* 57: 27–44
- Wend S, Dal Bosco C, Kaempfer MM, Ren F, Palme K, Weber W, Dovzhenko A, Zurbriggen MD (2013) A quantitative ratiometric sensor for time-resolved analysis of auxin dynamics. *Sci Rep* 3: 2052
- Wittig I, Braun HP, Schagger H (2006) Blue native PAGE. *Nat Protoc* 1: 418–428
- Wu G, Otegui MS, Spalding EP (2010) The ER-localized TWD1 immunophilin is necessary for localization of multidrug resistance-like proteins required for polar auxin transport in *Arabidopsis* roots. *Plant Cell* 22: 3295–3304
- Wu G, Lewis DR, Spalding EP (2007) Mutations in *Arabidopsis* multidrug resistance-like ABC transporters separate the roles of acropetal and basipetal auxin transport in lateral root development. *Plant Cell* 19: 1826–1837
- Xu J, Scheres B (2005) Dissection of *Arabidopsis* ADP-RIBOSYLATION FACTOR 1 function in epidermal cell polarity. *Plant Cell* 17: 525–536
- Xu M, Zhu L, Shou HX, Wu P (2005) A PIN1 family gene, OsPIN1, involved in auxin-dependent adventitious root emergence and tillering in rice. *Plant Cell Physiol* 46: 1674–1681
- Yang H, Murphy AS (2009) Functional expression and characterization of *Arabidopsis* ABCB, AUX 1 and PIN auxin transporters in *Schizosaccharomyces pombe*. *Plant J* 59: 179–191
- Zadnikova P, Petrasek J, Marhavy P, Raz V, Vandenbussche F, Ding Z, Schwarzerova K, Morita MT, Tasaka M, Hejatkó J et al (2010) Role of PIN-mediated auxin efflux in apical hook development of *Arabidopsis thaliana*. *Development* 137: 607–617
- Zahniser NR, Doolen S (2001) Chronic and acute regulation of Na⁺/Cl⁻-dependent neurotransmitter transporters: drugs, substrates, presynaptic receptors, and signaling systems. *Pharmacol Ther* 92: 21–55
- Zhu J, Bailly A, Zwiewka M, Sovero V, Di Donato M, Ge P, Oehri J, Aryal B, Hao P, Linnert M et al (2016) TWISTED DWARF1 mediates the action of auxin transport inhibitors on actin cytoskeleton dynamics. *Plant Cell* 28: 930–948
- Zourelidou M, Absmanner B, Weller B, Barbosa IC, Willige BC, Fastner A, Streit V, Port SA, Colcombet J, de la Fuente van Bentem S et al (2014) Auxin efflux by PIN-FORMED proteins is activated by two different protein kinases, D6 PROTEIN KINASE and PINOID. *eLife* 3: e02860



License: This is an open access article under the terms of the Creative Commons Attribution-NonCommercial-NoDerivs 4.0 License, which permits use and distribution in any medium, provided the original work is properly cited, the use is non-commercial and no modifications or adaptations are made.